Rev.Adv.Mater.Sci. 25 (2010) 113-121

# USE OF TEM KIKUCHI BANDS FOR MICROSTRUCTURE AND THERMAL STABILITY STUDY OF ECA PRESSED AA1200 VIA ROUTES A, C, Bc

**M. Cabibbo**

Department of Mechanical Engineering, Marche Polytechnic University, Via Brecce Bianche, 60131-Ancona, Italy

*Received: September 17, 2009*

**Abstract.** The evolution of the microstructure during ECAP depends upon the shearing deformation paths introduced into the material. Some authors, using selected-area electron diffraction, reported an effectiveness of cell (low-angle boundaries) evolution toward high-angle boundaries on the order Bc > C > A. This study focused on the cell and grain boundary evolution of an AA1200 during ECAP, up to a true strain of $\varepsilon$=8.64, in routes A, C, and Bc. TEM Kikuchi bands were used for the quantitative evaluation of boundary misorientation. A different hierarchy of cell evolution to grains was found, and this was as C > Bc > A; while in terms of reducing grain size, the route efficiency remained as Bc $\geq$ C > A. Thermal stability of the severely deformed alloy was studied by annealing the alloy at 0.5, 0.6, 0.7 $T_M$ for 2 hrs. It appeared that, even if route Bc is the one involving a faster microstructure grain refining, route C is likely to be the most stable upon reheating.

## 1. INTRODUCTION

Methods for obtaining ultra-fine-grained materials are currently attracting a great deal of attention. This is primarily due to the superior mechanical and physical properties the ultra-fine-grained materials exhibit such: increased strength, hardness, wear resistance [1,2]. Severe plastic deformation (SPD) techniques are able to produce bulk materials with fine grained structure [3]. Among the SPD techniques, equal channel angular pressing (ECAP) under particular circumstances is able to give grain sizes in the submicrometre range of ~400-800 nm [3-6].

In ECAP, the microstructure evolution with accumulative strain can be easily driven and optimized by modifying the specific shear deformation path. In fact, the microstructure evolution during ECAP is directly linked to a complex evolution of dislocation networks. That is, dislocation recombination and annihilation phenomena drive the microstructure modification to a quick and effective grain refinement. The way the billet is repetitively introduced into the L-shaped channels of the die determines the specific shear deformation path. Thus, the billet can be introduced into the die with no rotation between passes (unidirectional straining path – route A). Alternatively, billet can be introduced by rotating it of

Corresponding author: M. Cabibbo, e-mail: m.cabibbo@univpm.it

180 deg between passes (route C), or with a rotation of +90 deg in the same direction (route Bc) [8-12]. Other routes are known in literature, but for a sake of simplicity here are mentioned only the ones used in this study.

To date, a number of researchers have studied different aspects of the specific cell and grain evolution under different strain paths (routes) with different techniques [8-12]. For instance, in a study of pure aluminium, deformed at room temperature by a 90° equal-channels die, to a strain of 4, Iwahashi *et al*. [6,11] reported that the effectiveness of cells to evolve most rapidly into an array of high angle boundaries (HABs) is on the order Bc > C > A. They also reported route Bc to be the most effective route for producing equiaxed fine grain structure with HABs. In route A, a large portion of high angle boundaries (HABs) is generated, route C generates cycles of like deformation at each 2*N* passes, cycle of deformation extended to 4*N* passes in route Bc. Upon these considerations, the grain refining is expected to be less effective in routes Bc and C, compared to route A. Route Bc appears to be preferable to route C as it does not induce any deformation in the plane normal to the pressing direction [8]. Route Bc is effective in refining the microstructure, because four sets of shear bands are introduced into the material at each 4*N*-cycle. In route A, the shear bands, formed in the second pass, intersect the billet axis of symmetry at an angle of 45 deg, while the shear bands that formed in the first pass changed orientation to an angle of about 20 deg to the billet axis. The same procedure repeats at the following passes and continuously transforms the previous shear bands into an elongated grained structure along the flow direction. Apart from the shear deformation paths to which the material is subjected, Zhu and Li [8,12] showed that the die L-shaped corner plays a key role in determining which route is likely to more effectively generate HAB into the material microstructure. Thus they reported route Bc as the most effective deformation route for grain refinement in the case of a 90 deg L-channel die corner die, while route A as most effective when using a 120 deg die.

Whatever the route used, grains subdivide by the effect of newly introduced HABs on finer and finer length-scales, until ultimately a limit is reached where the HAB spacing converges with the cell size [13]. As a consequence, the boundary evolution proceeds from cells that have only cells as nearest neighbours towards cells having both grains and cells as nearest neighbours [14]. Average spacing between dislocation boundaries (cells) is a common microstructure parameter in deformed materials due to its inverse relationship with flow stress, as amply documented in the literature [15]. Studies of misorientation angles and of the early cell (often called subgrain) formation process are less investigated (e.g. [1,16-18]). Among these, very few papers reported TEM systematic studies on LAB and HAB misorientation evolution with strain for different strain paths [7,16,18-20]. These studies mainly focused on the correlation between deformation path and the resulting microstructure. The present work reports a TEM characterization of the evolution of LAB and HAB misorientation with accumulative strain. Kikuchi bands were used to quantitatively estimate the boundary misorientation, and then to measure cell and grain size.

An important feature concerning the ultra-fine-grained structure of metals, which has always to take into consideration, is the thermal stability of the severely deformed microstructure. That is, for a mechanical point of view, refined microstructures must retain their sub-micrometric structure upon heating at least up to 0.5 $T_M$ (where $T_M$ is the alloy melting temperature). Several studies have reported thermal stability and superplasticity behaviour of ECA pressed dispersoid-containing aluminium-magnesium alloys, showing a rather good thermal stability due to the presence of the Sc-dispersoids [21-23]. With this respect, Langdon *et al.*, in several studies [23-25], reported that a refined microstructure has a mechanical meaningful application only if it is retained (i.e. no recrystallization occurs) upon heating. It is straightforward that there will be a temperature threshold-like limit. This temperature will depend on the specific alloy (in the present case, aluminium alloy), the level of severe plastic deformation, and the thermo-mechanical processes to which the material is subjected.

In this study, the microstructure of the alloy subjected to ECAP, via different strain paths (routes A, C and Bc), up to a strain of e=8.64, was quantitatively characterized using transmission electron microscopy. Thermal stability studies were carried out for three different temperatures (0.5 $T_M$, 0.6 $T_M$, 0.7 $T_M$) in all the three routes: A, C, and Bc.

## 2. EXPERIMENTAL DETAILS AND METHOD

For this study a commercially pure aluminium (AA1200: 0.7Si, 0.3Fe, 0.1Zn, 0.03Cu, 0.02Mn, wt.%) was used. The material was machined to rod-shaped bars 10 mm in diameter and 100 mm in length, and then homogenised (540 °C / 4 h). The

microstructure of the bars was homogeneous with average grain size of 330 μm. Bars were subjected to severe plastic deformation by ECAP at room temperature with pressing forces ranging 20 to 70 kN and speed of 4 mm $min^{-1}$. ECAP was carried out using an open die whose two parts were bolted to give a single internal L-channel of cylindrical shape. The two cylindrical channels intersect at an angle $\Phi = 90$ deg and a curvature $\Psi = 20$ deg with equal cross section of $10 \times 10$ $mm^2$. This die configuration induces to the specimen a true strain of $\varepsilon = 1.08$ at each pass [6]. The alloy was subjected to three different routes: A, uniaxial straining, C, reverse straining of 180 deg at each pass, and Bc, +90 deg rotation at each consecutive pass.

Microstructure inspections of the ECAP specimens were carried out using a transmission electron microscope. TEM specimens were ground to a thickness of about 170 μm and then surfaces were chemical etched with a solution of perchloric acid ($HClO_4$) in methanol at room temperature for few minutes. Samples were sectioned along the *Z*-plane [9]. Thin discs were extracted from the TEM specimens, along the central zone of the *Z*-plane, and prepared to the last stage using electro-polishing at -40 °C, 18 V with a solution of 30 pct nitric acid ($HNO_3$) and 75 pct methanol ($CH_3OH$). The *Z*-plane was keep as inspection plane in all the three routes used in this study. Thus, in route A and C sectioning was constantly performed along the longer axis of symmetry of the billet out of a plane containing the pressing and transverse directions. In route Bc, sectioning of the samples was performed following the +90 deg billet rotation at each ECAP pass. Thus, considering the literature definition, inspections were carried out in a sequence: $+Z$, $-Y$, $-Z$, $+Y$.

TEM discs were examined in a PHILIPS CM-200™ equipped with a double-tilt specimen holder, operated at 200 kV.

The angle $\phi$ of boundary misorientation was measured either form Kikuchi patterns [18,19,26] or from Moiré fringes [27]. More than 250 boundaries were measured per strain level for each of the three routes. The orientation of the different cells were measured by taking a cell as reference and calculating the relative misorientation of the different surrounding crystals. The misorientation matrix is thus as $R_{CR} = R_{PR} \times R_{CP}$, where $R_{CP}$ is the matrix of the angles between the crystal and the electron beam, and $R_{PR}$ the matrix of the angles between the reference crystal and the beam direction (which is not necessarily at a low-indexed zone axis). Moiré fringes were evaluated, instead of Kikuchi analysis, for those boundaries showing them, and typically in cell boundary misorientation $\phi < 2°$. The angular measurement was carried out by counting the number of Moiré dark-bright pairs, *D*, directly on stage. The corresponding misorientation across the boundary is then determined as $\phi = 2^{-0.5}\, a/D$, where *a* is the crystal lattice spacing [18,27].

Average cell, λ, and grain, *d*, spacing between boundaries was determined using test lines drawn on TEM micrographs at equal distance parallel and perpendicular to the direction of cell elongation. Due to the microstructure inhomogeneity induced by the shear deformation throughout the material, the regions from which the quantitative misorientation evaluation was performed were selected to be representative of the microstructure features. Thus, for each experimental condition, at least three sets of measurements were performed from within the shear banding zones and form within zones outside these regions.

Polarized optical microscopy (POM) was carried out on central sections along the Z-plane. Surfaces were ground and etched using the same methods followed for the TEM specimens. Mean grain size was measured using parallel test lines drawn on the POM micrographs.

## 3. RESULTS AND DISCUSSION

Fig. 1 shows the cell structures after four and height ECAP passes. Grain subdivision starts first at the largest length scale (i.e. with primary deformation bands), and then, moves down to the next available level (grain walls and eventually cell walls) with accumulative strain. A banded structure of elongated cells / grains develops on route A (Figs. 1a and 1d). This is due to the monotonic increase of the shear deformation induced in this route. After the first pass, the shear bands form an angle of ~45 deg with respect to the pressing direction. As the strain accumulates, the deviation of shear band inclination to the pressing direction progressively rises. By contrast, cells / grains morphology is essentially restored at every 2 and 4 passes, in route C and Bc, respectively. As a consequence, cell and grain structures look much more equiaxed with accumulative strain in these two deformation routes (Figs. 1b, 1c, 1e, 1f). In route Bc, the homogeneity of the cells is evident at both strain levels ($\varepsilon = 4.32$ and $\varepsilon = 8.64$).

Fig. 2 gives the distribution of misorientation, $\phi$, in all the three routes. After the first pass, 75 pct of the boundaries have low-angle character ($\phi$<15 deg). Distribution in route A (Fig. 2a) appears to evolve

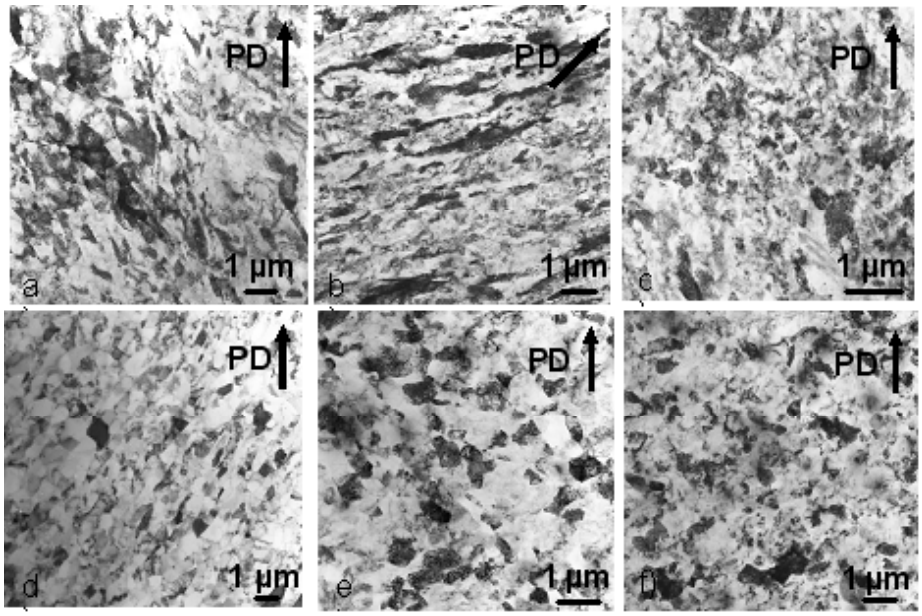


**Fig. 1.** TEM images of cell structure after 4 and 8 passes for routes A (a), (d), route C (b), (e), and route Bc (c), (f). The pressing direction (PD) is also reported.

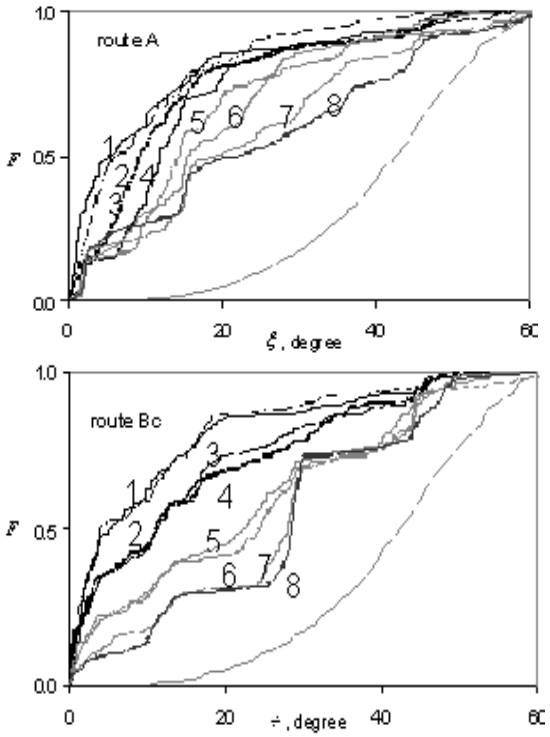


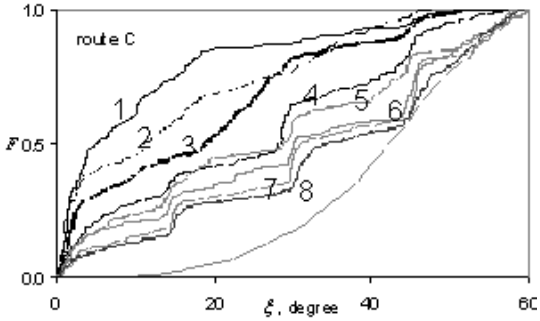


**Fig. 2.** Cumulative frequency distribution of misorientation $\phi$ in the three routes: A (a), C (b), and Bc (c). Every plot is labelled with the corresponding number of ECAP passes. The Mackenzie distribution is reported as dotted line plot.

from low-angle boundaries to high-angle boundaries quite rapidly. After a strain of $\varepsilon = 3.24$ (3rd pass), a step at ~ 2 deg starts to develop and consolidate in the distribution. A second step at misorientation range of $\phi$ between 15 and 18 deg starts to develop at a strain $\varepsilon = 4.32$ (4th pass), while a step at $\phi = 45$ deg only appears at $\varepsilon = 8.48$ (8th pass). The cumulative misorientation slowly approach to the Mackenzie distribution but remains quite distant from it even at the maximum strain. On the other hand, route C distribution (Fig. 2b) approaches to the Mackenzie distribution much quickly, and it starts

showing random distribution for misorientation angles f > 40 deg, at the 8th pass. Thus, the generation of high-angle boundaries is, to some extent, slower. Distribution of the different strain levels appear more separate and shows step-like misorientation increment from a strain level of E = 3.24 (3rd pass). Misorientation distribution of route Bc (Fig. 2c) is not dissimilar to the one of route C. Yet, some relevant differences can be highlighted. At the even-numbered passes 2*n* the distribution appears quite similar to that of the preceding odd-numbered passes 2*n* -1. Moreover, the rate of evolution in odd-numbered passes is higher than in the even-numbered passes, where the distribution remains practically constant or, in some cases, it slightly increases. At the maximum strain of $\varepsilon$ = 8.64, the fraction of the low-angle boundaries, $F(\phi$ < 15 deg), is still 30 pct and, as a matter of fact, it is still higher than the expected random orientation (Mackenzie). Steps in the curves indicate the presence and evolution of a pronounced texture in the observed regions [28]. Yet, the limited area of investigations makes not possible to use the existing steps in the misorientation distributions for a reliable interpretation of the texture evolution with accumulative strain.

Fig. 3 has been derived from Fig. 2 and reports the fraction of boundaries grouped in 15 deg ranges of misorientation: $\phi$ < 15 deg - Low Angle Boundaries (LABs), 15 $\leq \phi$ < 30 deg - Low High Angle Boundaries (LHABs), 30 $\leq \phi$ < 45 deg - Medium High Angle Boundaries (MHABs), $\phi \geq$ 45 deg - Very High Angle Boundaries (VHABs). A rather monotonic decrease of LABs is common to all the three routes. In particular, the shrinking of low-angle fraction with strain in route Bc is characterized by a clear step-like behaviour. At every 2*n* passes, the fraction is essentially equal to the previous 2*n* -1 pass. In route A, a relevant increase of the LHAB, MHAB, and VHAB is only observed at a strain of $\varepsilon$ = 5.40 (after 5 passes). In route C, in spite of a peak at 40 pct of the LHAB at $\varepsilon$ = 3.24, LHAB and MHAB do not show a relevant increment with strain, the VHAB population continuously increases with strain from 6 pct, at $\varepsilon$ = 1.08 (1 pass) to 42 pct at $\varepsilon$ = 8.64 (8 passes). In route Bc, the population reduction of the LAB contributes to a slow, but continuous, unit increment of all the HAB population (LHAB, MHAB, and VHAB) with similar rate. The unit increment of all the three HAB ranges is rather modest accounting in some cases to a two-fold rise after 8 passes compared to the first pass fraction. This reflects the still relatively high fraction of the LABs at the maximum strain of $\varepsilon$ = 8.64, in all the three routes. Nevertheless, the fraction of the LHAB is constantly the highest among the group of the HABs with the only exception of route C, starting from the 5th pass. That is, LABs evolve into HABs rather gradually and the depletion in the LAB distribution with strain essentially contribute to the population of the LHABs. These progressively evolve into MHAB and eventually to VHAB. Route Bc shows a

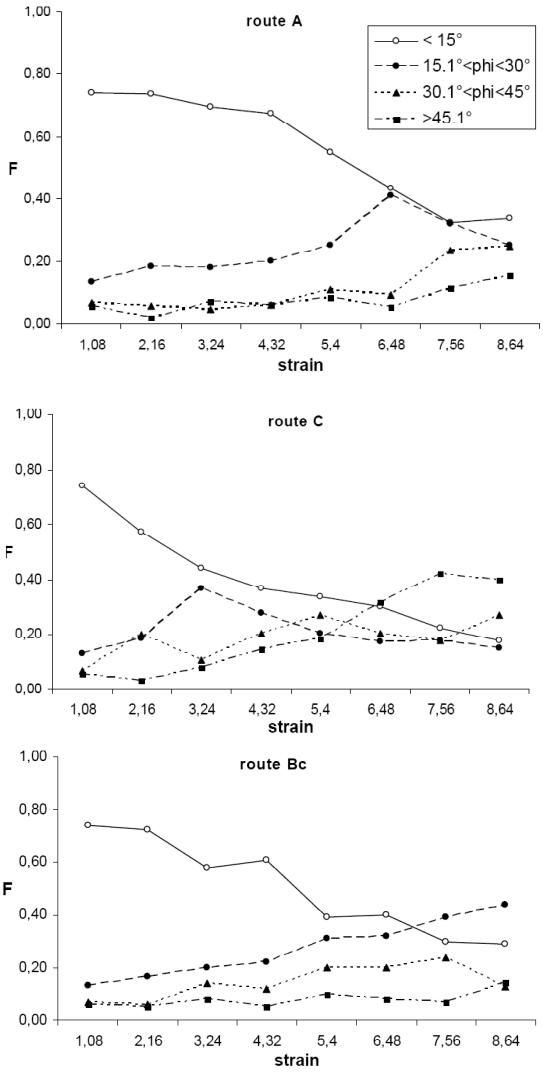


**Fig. 3.** Frequency of misorientation f in different 15 deg interval ranges. Open-circle datapoint: Low Angle Boundaries (LABs, $\phi$ < 15 deg); solid-circle datapoints: Low High Angle Boundaries (LHABs, 15 deg $\leq \phi$ < 30 deg); solid-triangle datapoints: Medium High Angle Boundaries (MHABs, 30 deg $\leq \phi$ < 45 deg); solid-square datapoints: Very High Angle Boundaries (VHABs, $\phi \geq$ 45 deg). Route A (a), C (b), and Bc (c).

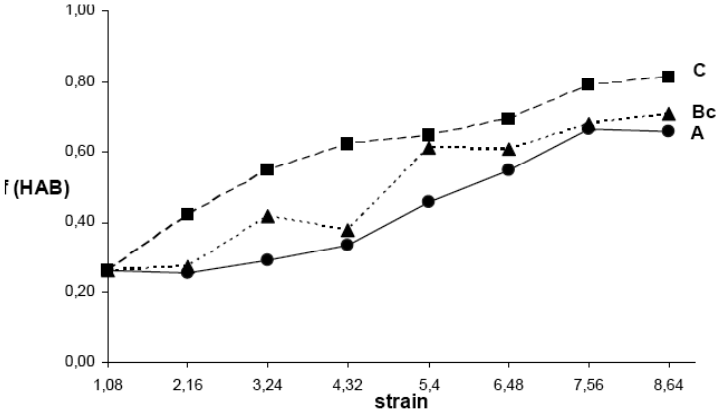


**Fig. 4.** Mean fraction of HAB, $\phi_{HAB}$, as a function of ECAP strain for routes A, C, and Bc.

linear and almost monotonic growth of the faction of all the three HAB ranges with strain. It is likely that the route Bc, among the three routes here considered, drives the generation of the HAB with strain in the most progressive and effective manner, from the LAB to LHAB, MHAB and then VHAB.

Shear plane changes at each ECAP pass, induced in route Bc, are likely to favour shear band intersections, which develop a near spatially uniform network in the material, and consequently leads to a higher efficiency in HAB generation. Furukawa *et al*. [29], in an Al-Mg alloy, suggested that a wide angular range of slip traces might favour the formation of fine equiaxed grains. It may account for the present observations, that among the three routes studied, the grains developed in route Bc have the most equiaxed shape and the smallest size.

The mean fraction of HABs, $f_{HAB}$, as a function of ECAP strain is shown in Fig. 4. At the maximum strain of $\varepsilon = 8.64$, $f_{HAB}$ reaches 66, 81 and 71 pct, in route A, C and Bc, respectively. The unit increment of $f_{HAB}$ shows some differences among the three routes. Route A is the only one clearly showing a S-shape curve, which is likely to mean that a saturation limit of HAB is reached at $\varepsilon = 8.64$. The plot of route C constantly stays above the other two curves meaning a faster generation of HAB since the earliest strain levels. The plot of route Bc shows an alternate distribution of datapoints across the intercept trend curve, which reflects the different dislocation accumulation and annihilation phenomena occurring at each 2*n* pass respect each previous 2*n* -1 pass. Among the three different routes, at the intermediate strain level, $\varepsilon = 4.32$, the material processed via route A and route Bc contained the lowest density of high angle boundaries with a high-angle grain boundary fraction of only 33 pct, while route C reached an almost double fraction, 63 pct. At the maximum strain, $\varepsilon = 8.64$, the HAB fraction in route A is of 66 pct, in route C is higher (81 pct), and intermediate in route Bc (71 pct). Thus, this figure invariably shows that the efficiency of generating HAB is as: C > Bc > A.

In other studies [11] the efficiency of generation of HAB was reported to be as Bc > C > A, which would mean a much larger HAB fraction, $f_{HAB}$, in route Bc respect to the present findings. This discrepancy is believed to be attributed to a quite different evaluation method for the HAB fraction evaluation out of their boundary misorientation measurements. In the present study, a systematic TEM study was carried out using a quantitative method through the Kikuchi bands misorientation measurement. This method is far more reliable than other semi-quantitative, or even qualitative, methods. Other quantitative techniques have also been developed and now commonly used for these purposes. Among these, the FEGSEM Electron-Back-Scattered Diffraction (EBSD) method is quite attractive and time-saving. Nevertheless, results obtained by using EBSD suffer from an overestimation of HABs as the misorientation resolution lies within 2 – 3 deg and, more important, the boundaries showing Moiré fringes can not be detected. Moiré fringes that were much more abundant in route Bc compared to route C microstructure. This feature can explain the discrepancy of the present findings with data published by Huang, Cao, and others using FEGSEM EBSD [7,19,30-32].

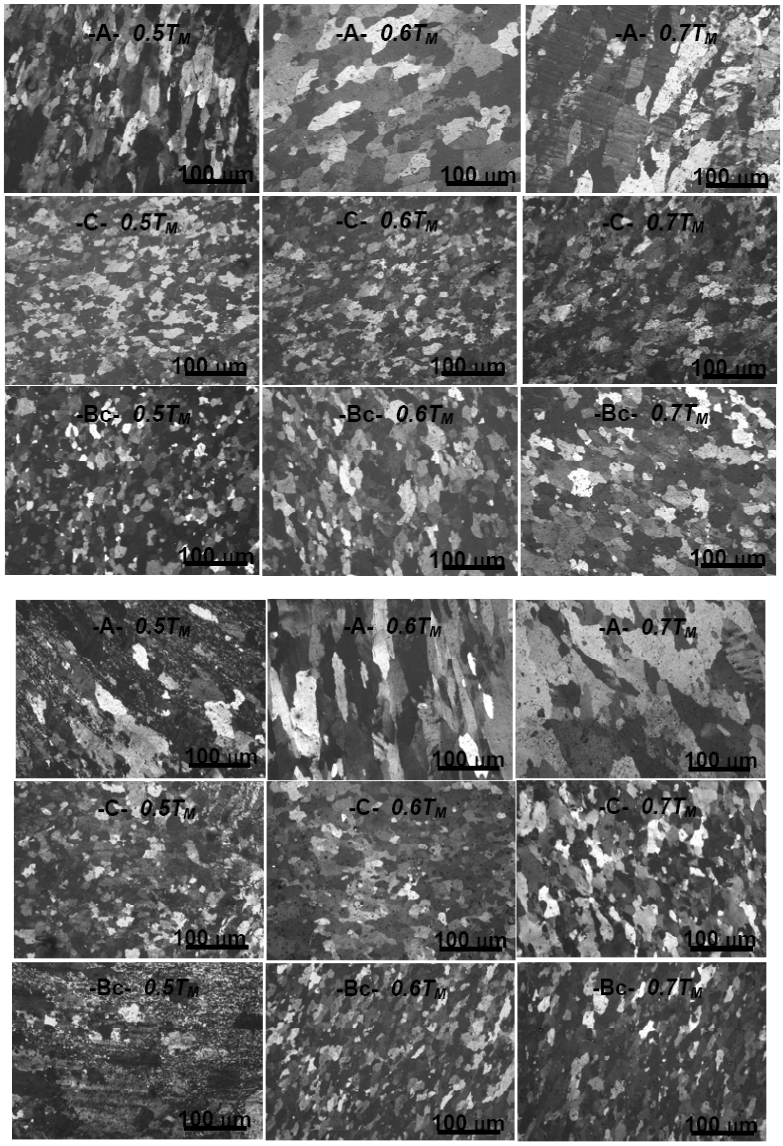


**Fig. 5.** Representative POM images of the three routes after the post-ECAP annealing. (a): microstructure after 4 passes and annealing at: 0.5 $T_M$ (330 °C), 0.6 $T_M$ (390 °C), and 0.7 $T_M$ (430 °C). (b): microstructure after 8 passes and annealing at same temperatures.

In order to test the thermal stability, the severely deformed alloy was annealed at 0.5,0.6, and 0.7 $T_M$ / 2 h (where $T_M$ = 933K is the alloy melting temperature). Figs. 5a and 5b show POM of the post-ECAP annealed alloy, after the 4$^{th}$ and 8$^{th}$ pass, respectively. The 4 passes-ECAP and annealed microstructures show a grain coarsening with annealing temperatures. In particular, route A experienced the most dramatic grain coarsening with a microstructure almost no longer showing traces of the fine-grain structure obtained during ECAP. The annealed microstructures of the 8 ECAP passes condition at 0.5 $T_M$ show large portion of ultra-fine grained structure, especially for route A and Bc. As the annealing temperature rise, grain coarsen to a great extent in route A, while route Bc still shows a reasonable fine grain structure, with limited coarsening. The case of route C is somewhat different. The $\varepsilon$ = 8.64 + 0.5 $T_M$ annealed conditions showed a grain structure coarser in the average, but much more homogeneous, respect route A and Bc. The grain structure remains essentially stable with the anneal-

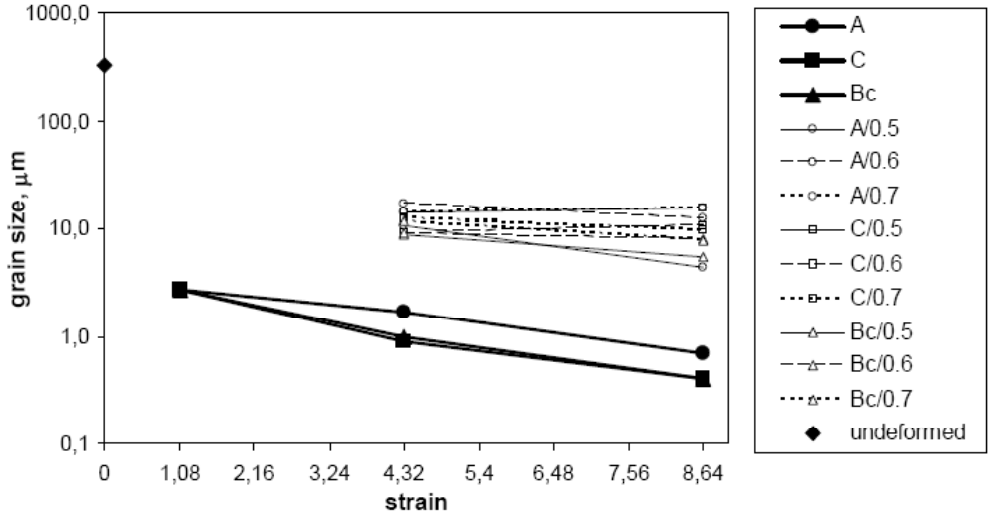


**Fig. 6.** Grain size, *d*, after ε = 4.32 (4 passes) and ε = 8.64 (8 passes), and after post-ECAP annealing to 0.5, 0.6, and 0.7 $T_M$. mean grain size of the undeformed homogenised alloy condition is also reported.

ing temperature. That is, the POM showed grains coarsened upon annealing at 0.5 $T_M$, but the grains did not further coarsen significantly at 0.6 and 0.7 $T_M$, either in the 4 and 8 passes conditions.

Fig. 6 shows the evolution of the grain spacing, *d*, either for the ECAP and post-ECAP annealed conditions. Mean grain size of the ECAP three routes monotonically reduces from 2.7 mm, after the first pass (ε = 1.08), down to ~700 nm in route A, and ~400 for routes C and Bc after 8 passes (ε = 8.64). Upon reheating to temperatures ranging 0.5-to-0.7 $T_M$, grain size practically raised by an order of magnitude, irrespective of the route used. Even if in any case the mean grain size coarsened to the level of the undeformed condition (*d* = 330 μm), the microstructure after annealing can not longer be considered as ultrafine or sub-micrometric. A static recrystallization occurred during annealing. The recrystallization rate is directly driven by the amount of severe plastic deformation the material underwent during ECAP and by the following annealing temperature. The ultra-fine grained structure instability upon annealing is certainly due to the absence of any kind of dispersoids or fine precipitates in the alloy. The only significant results concerns the route C where microstructure revealed a grain size homogeneity over the three annealing temperatures and the two strain levels (ε = 4.32 and ε = 8.64).

## 4. CONCLUDING REMARKS

This study focused on the role of three different ECAP strain paths, route A, C, and Bc, in the microstructure evolution prior and after annealing at 0.5, 0.6, 0.7 $T_M$ ($T_M$: alloy melting temperature). An AA1200 and a Φ = 90 deg ECAP die were used. Boundary misorientation has been successfully characterized using Kikuchi bands and Moiré fringes on TEM. These techniques, although time-consuming, are far more reliable than other automated techniques, such as the FEGSEM OIM which also use Kikuchi bands for the boundary misorientation measurements. The lower boundary misorientation accuracy limit was of ϕ = 0.1 deg. The role of the boundary showing Moiré fringes was also clarified and it is believed to be the key aspect for the different route efficiency hierarchy found in the present work compared to some other literature findings.

It was found thus that:

(i) in terms of generation of HABs, the route efficiency is C > Bc > A;

(ii) in terms of reducing grain size, the route efficiency is Bc > C > A;

Results of the material subjected to annealing showed that:

(iii) static recrystallization occurred in all the three routes. In particular, route C showed rather good grain size uniformity over the annealing temperatures and the strain levels.

## ACKNOWLEDGEMENTS

The author acknowledges Mr. D. Ciccarelli for the POM specimen preparation.

## REFERENCES

[1] P.B. Prangnell and J.R. Bowen, In: *Proc. UFG materials-II*, ed. by Y.T. Zhu, T.G. Langdon, R.S. Mishra, S.L. Semiatin, M.J. Saran and T.C. Lowe (TMS, 2002), p. 89.
[2] S.D. Terhune, D.L. Swisher, K. Oh-Ishi, Z. Horita, T.G. Langdon and T.R. McNelley // *Metall. Mater. Trans.* **33A** (2002) 2173.
[3] R.Z. Valiev and T.G. Langdon // *Progr Mater Sci.* **51** (2006) 881.
[4] K. Nakashima, Z. Horita, M. Nemoto and T.G. Langdon // *Acta Mater.* **46** (1998) 1589.
[5] A. Shan, I.G. Moon and J.W. Park // *J. Mater. Proc. Techn.* **122** (2002) 255.
[6] Y. Iwahashi, J. Wang, Z. Horita, M. Nemoto and T.G. Langdon // *Scripta mater.* **35** (1996) 143.
[7] K.S. Raju, M.G. Krishna, K.A. Padmanabhan, K. Muraleedharan, N.P. Gurao and G. Wilde // *Mater. Sci. Eng.* **A491** (2008) 1.
[8] Y.T. Zhu and T.C. Lowe // *Mater. Sci. Eng.* **A291** (2000) 46.
[9] M. Furukawa, Y. Iwahashi, Z. Horita, M. Nemoto and T.G. Langdon // *Mater. Sci. Eng.* **A257** (1998) 328.
[10] T.G. Langdon // *Mater Sci Eng.* **A462** (2007) 3.
[11] Y. Iwahashi, Z. Horita, M. Nemoto and T.G. Langdon // *Acta Mater.* **46** (1998) 3317.
[12] S. Li // *Scripta mater.* **60** (2009) 356.
[13] H.J. McQueen, N.D. Ryan, E.V. Konopleva and X. Xia // *Can Metall Quarterly* **34** (1995) 219.
[14] D.A. Hughes, Q. Liu, D.C. Chrzan and N. Hansen // *Acta Mater.* **45** (1997) 105.
[15] N. Hansen and D. Juul Jensen // *Acta Metall*. **40** (1992) 3265.
[16] S.C. Baik, Y. Estrin, H.S. Kim and R.J. Hellmig // *Mater. Sci. Eng.* **A351** (2003) 86.
[17] P.L. Sun, P.W. Kao and C.P. Chang // *Scripta mater.* **51** (2004) 565.
[18] M. Cabibbo, W. Blum, E. Evangelista, M.E. Kassner and M.A. Meyers // *Metall Mater Trans.* **39A** (2008) 181.
[19] M. Reihanian, R. Ebrahimi, M.M. Moshksar, D. Terada and N. Tsuji // *Mater. Character.* **59** (1997) 105.
[20] M. Cabibbo and E. Evangelista // *J. Mater. Sci.* **41** (2006) 5338.
[21] J.L. Ning and D.M. Jiang // *Mater Sci Eng*. **A452-3** (2007) 552.
[22] A. Vinogradov, A. Washikita, K. Kitagawa and V.I. Kopylov // *Mater Sci Eng.* **A349** (2003) 318.
[23] S. Komura, M. Furukawa, Z. Horita, M. Nemoto and T.G. Langdon // *Mater. Sci. Eng.* **A297** (2001) 111.
[24] S. Lee, M. Furukawa, Z. Horita and T.G. Langdon // *Mater Sci Eng.* **A342** (2003) 294.
[25] C. Xu, M. Furukawa Z. Horita and T.G. Langdon // *Acta Mater.* **51** (2003) 6139.
[26] Q. Liu, X. Huang and M. Yao // *Ultramicroscopy.* **41** (1992) 317.
[27] D.B. Williams and C.B. Carter, *Transmission Electron Microscopy; Diffraction* (Plenum Press, New York, NY, 1996).
[28] M. Cabibbo, E. Evangelista and C. Scalabroni // *Micron.* **36** (2005) 401.
[29] M. Furukawa, Z. Horita, M. Nemoto, R.Z. Valiev and T.G. Langdon // *Acta Mater.* **44** (1996) 4619.
[30] J.C. Huang, I.C. Hsiao, T.D. Wang and B.Y. Lou // *Scripta Mater.* **43** (2000) 213.
[31] Y. Huang and F.J. Humphreys // *Mater. Charact.* **47** (2001) 235.
[32] W.Q. Cao, A. Godfrey, W. Liu and Q. Liu // *Mater. Sci. Eng.* **A360** (2003) 420.